SP-230—24

Debonding in FRP-Strengthened Flexural Members with Different Shear-Span Ratios

by Z. Wu and S. Hemdan

Synopsis: The use of fiber reinforced polymers (FRP) as external reinforcement to the tension face of concrete members has bean accepted as an effective mean of strengthening and retrofitting aging and deteriorated structures. One of the problems which limit the full utilization of the material strength is the premature failure due to debonding. In this study a special attention is paid to investigate the effect of the shear-span ratio on the debonding due to flexural cracks of concrete in FRP-retrofitted beams. Based on finite element analysis and nonlinear fracture mechanics, the debonding behavior of FRP-retrofitted beams with different shear-span ratios was investigated. The initiation of macro debonding of each beam was recorded and main factors affecting the effective bonding length were discussed. It is concluded that shear-span ratio has an insignificant effect on the initiation of macro debonding while it greatly affects the effective bonding length.

Keywords: debonding; effective bonding length; fiber reinforced polymers (FRP); shear-span ratio

Zishen Wu is a professor in the department of Urban & Civil Engineering at Ibaraki University, Japan. He received his BS and MS from the Southeast University, China in 1983 and 1985, respectively and his PhD from Nagoya University, Japan in 1990. His research interests include computational fracture and failure mechanics of composite materials and structures, maintenance engineering, structural health monitoring, intelligent and security engineering.

Said Hemdan is a PhD candidate in the department of Urban & Civil Engineering at Ibaraki University, Japan. He received his BS and MS from Assiut University, Egypt in 1996 and 2001 respectively. His research interests include nonlinear finite modeling and optimization design of reinforced concrete members retrofitted by fiber reinforced polymers.

INTRODUCTION

The use of fiber reinforced polymers (FRP) as an innovative method for retrofitting concrete members in both shear and flexure has been developed during the last two decades to replace the conventional methods such as steel plates. Although fiber reinforced polymers (FRP) have many advantages such as high efficiency, low weight/strength ratio, and ease of application, they still have their own drawbacks. One of the most popular problems accompanied with the use the bonded FRP sheets is the premature failure due to debonding which limits the complete utilization of the material strength. Over the last several years, great efforts have been paid to understand the debonding phenomena and to develop methods on evaluating the debonding load-carrying capacities.

Two different types of debonding were observed, the first type is debonding at the cut-off point of FRP caused by stress concentration as investigated by many researchers such as (Roberts, 1989; Ziraba et al., 1994; Malek et al., 1998; Ahmed et al., 2000). This type of debonding is dominant in case of FRP/steel plates. The another type of debonding which is observed to be dominant in the case of using FRP sheets with relatively thin thickness is that debonding initiates from the end of flexural cracks near the region of the maximum bending moment which is usually called intermediate crack-induced debonding. The intermediate crack-induced debonding has attracted many researchers to investigate it (e.g. Triantafillou, 1992; Täljstin, 1996; Wu et al. 1997; Bizindavyi et al., 1999; Yoshizawa et al., 2000; Sato et al., 2000; Lorenzis et al., 2001; Chen & Teng., 2001; Niu et al. 2002; and Wu & Yin, 2002). Täljstin (1997) presented the use of a linear and nonlinear fracture mechanics approach for the plate bonding technique. The expressions on stress transfer and mode II fracture are derived analytically for a simplified shear stress-deformation curve. Yoshizawa et al. (2000) found that the local shear stress distribution, effective transfer length, initiation and propagation of debonding could be well represented by the bi-linear model shown in Figure 4. They also, identified an average bond-slip relationship with local bond strength of 8 MPa and fracture energy of 1.2 MPa mm. Niu et al. (2002) performed a parametric study to illustrate the effect of the adhesive properties on the behavior of the FRP retrofitted beams; they concluded that the interfacial fracture energy is the only

parameter to govern the ultimate load-carrying capacity. Chen and Teng (2001) assessed the performance of some of the available bond models and proposed a new model defined by combining fracture mechanics analysis with experimental evidence. Their model is a modification of the model proposed by Yuan and Wu (1999). Chen and Teng (2001) observed that the shear-slip behavior of plate concrete bonded joints may be well represented by a triangular shear-slip model similar to that shown in Figure 4. Because the relative slip at the peak shear is relatively too small when compared to the relative slip at failure, Chen and Teng (2001) suggested that a linear decreasing shear-slip model may be used. Their model uses the compressive strength of concrete instead of the shear-slip properties because accurate measurements of the later are practically difficult. Also, they took into consideration the width ratio of the bonded plate to the concrete member.

An important feature observed in many literatures is that there is a certain length beyond which any increase in the FRP bond length cannot increase the bond strength and hence can not contribute in the increase of the load-carrying capacity, this length is regarded as the effective bonding length. Extensive work has been done by Wu and his research group to illustrate the phenomena of debonding and the effect of cracks on the effective bonding length in a flexural concrete member. They concluded that the effective bonding length may be increased due to existence of cracks as compared with the effective transfer length determined without any crack in the simple shear test.

Based on the pre-mentioned studies and various relevant field applications, code provisions have been also issued in various countries: In the USA, ACI 440.2R-02 *Guide for the Design and Construction of Externally Bonded FRP Systems for Strengthening Concrete Structures* (ACI 2002) suggests a simple method for avoiding premature failure due to debonding in the anchorage zone and through all the interface length by limiting the allowable strain in the FRP to a value smaller than the FRP rupture strain. The method of the ACI is empirically and derived mainly from the experimental data.

Based on the analogy between the simple shear test without cracking and the RC beam behavior with cracking, the Japanese Code of Standards (JSCE Recommendations 2001) introduces an explicit method for checking the FRP strengthened beams against the premature failure due to loss of bonding. A double check procedure is suggested to ensure that no debonding occurs neither in the anchorage zone nor along the adhesive interface. JSCE suggested a procedure to calculate the flexural capacity and axial load-carrying capacity of members that fail due to peeling of the continuous fiber. Two main parameters are essential for the JSCE method: fracture energy which may be measured from the simple shear tests and the generalized effective bonding length in RC beam with cracking. Although JSCE suggests some equations for calculating the effective bonding length, these equations need to be developed to take into account the effect of more parameters such as shear-span ratio.

Fib bulletin 14 (2001) has a similar approach to the JSCE and states that stress check against delamination between two adjacent cracks can be carried out by limiting the FRP stress difference between the two cracks to a limited value. Also, Fib bulletin 14 (2001) provides relationships for estimating the average distance to be assumed between flexural cracks. The mechanical meaning of the Fib method is still unclear.

Evaluation of the aforementioned code provisions has demonstrated that no one of them is completely valid and can be used to describe debonding accurately (C. Faella at al. 2004). In addition, there are still some difficulties in estimating some of the needed parameters involved by the suggested equations such as crack spacing, fracture energy of the adhesive and effective bonding length. So, we still need to develop such equations to obtain a reliable one. In order to find a suitable relation for estimating the debonding failure capacity, basic factors affecting the effective bonding length as well as the effect of shear-span ratio on the debonding behavior are discussed in this paper.

RESEARCH SIGNIFICANCE

Debonding due to flexural cracks of concrete in FRP-retrofitted beams has been reported as a dominant mode of failure. Code provisions have been issued in various countries to give suggestions and recommendations to overcome this premature failure mode. JSCE suggested a procedure to calculate the flexural capacity and axial load-carrying capacity of members that fail due to peeling of the continuous fiber. Two main parameters are essential for the JSCE method: fracture energy which may be measured from the simple shear tests and the generalized effective bonding length in RC beam with cracking. Although JSCE suggests some equations for calculating the effective bonding length, these equations need to be developed to take into account the effect of more parameters such as shear-span ratio.

FINITE ELEMENT MODELING

A schematic drawing for the details of the simulated beams is shown in Figure 1. As it is clear, every beam is composed of three main parts: concrete, reinforcing bars and FRP sheets. For all cases, the beam cross section and reinforcement ratio were held constant, while the clear span was varied as which will be discussed later. Because we are using FRP sheets not the thicker FRP plates, so debonding of FRP sheets from the end of flexural cracks is expected to be the dominant failure mode. Therefore, to simulate the real response accurately, it is necessary to establish appropriate models for considering the crack propagation in concrete, bond-slip behavior between reinforcing bars and concrete and bonding behavior along the adhesive layer.

The discrete crack model is adopted here to simulate the initiation and propagation of cracks. It is assumed that flexural cracks are vertical along the whole depth of the beam and can develop only in the prescribed locations, no shear cracks are taken into consideration. According to Hillerborg et al. (1976), the linear softening curve shown in Figure2 is considered to model the mod I tension softening behavior of concrete. In this model, the cohesive crack, where forces are followed by a given

softening curve, is assumed to initiate if the tensile stress reaches the tensile strength *ft*. The macro crack, where no shear stress is transferred along the interface of crack, is formed when the energy required to create one unit area of crack is met. The fracture energy G_f^c is represented by the area below the curve. Unloading and reloading are modeled by a secant path. The values of *ft*= 3.0 MPa and G_f^c= 0.12 MPa mm were employed in this study. The bond-slip model proposed by Morita et al. (1967) is adopted to simulate the interfacial behavior between concrete and the deformed steel bars as shown in Figure 3. Unloading and reloading are modeled by a secant path, which means upon a slip reversal, a straight line back to the origin is followed.

A linear softening model shown in Figure 4 is adopted to simulate the mode-II fracture of the adhesive. This model is considered valid for simulating the bond behavior regardless whether debonding occurs within the interfacial concrete or through the adhesive layer. In this model, when the local bond stress attains the local bond strength τ_f, micro-debonding is initiated and followed by a decrease in the local bond stress until it becomes zero where macro-debonding is formed . The slope of the ascending branch represents the interfacial stiffness k_s, while the area under the curve represents the mode II fracture energy G_f^b. According to Yoshizawa et al. (2000), the values of τ_f, k_s, and G_f^b are chosen to be 8.0 MPa, 160 MPa/mm, and 1.2 MPa mm respectively as a set of reference values.

As described above, the tensile behavior of concrete is modeled using a discrete cracking model. On the other hand, the response of concrete in compression is modeled by Drucker-Prager perfect plasticity, where the internal friction angle is taken as 10^o. The compressive strength and the Young's modulus of concrete were chosen to be 40 MPa and 34.2 GPa respectively.

Steel reinforcing bars are considered as a linear elastic-perfectly plastic material, as shown in Figure 5. The slope of the curve represents the modulus of elasticity Es and the maximum stress represents the yield stress f_y. The elastic-perfectly plastic behavior is modeled by Von Mises yield criterion. The values of Es and f_y are chosen to be 210 GPa and 364 MPa, respectively. FRP sheets in general behave in linear elastic manner up to rupture. The modulus of elasticity and the tensile strength are chosen to be 230 GPa and 4.1 GPa, respectively.

The simply supported beam shown in Figure1 was simulated numerically. The small deformation theory is adopted, large deformations are not considered in the simulation. Due to symmetry, only half of the beam was solved with appropriate boundaries. Beams were solved under three point loading using displacement control. The concrete beam is modeled by 4-node plane stress elements, steel bars and FRP sheets are modeled by 2-node linear truss elements connected to concrete by zero-thickness line interface elements. The flexural cracks are modeled by zero-thickness line interface elements at a spacing of 40mm from the mid-span to the support of the beam. The crack spacing was chosen to be 40mm to cover a wide range of crack distributions, especially in the case of relatively longer spans.

NUMERICAL SIMULATION

As stated above, we are aiming mainly at clarifying the effect of the shear-span ratio on the debonding behavior in addition to investigating the parameters that affect the effective bonding length. To investigate the effect of the shear-span ratio on the debonding behavior, 5 beams of clear spans of 1800, 2400, 3000, 3600, and 4800 which are corresponding to shear-span ratios of 4.5, 6.0, 7.5, 9.0, and 12.0 respectively were solved. Each beam was retrofitted by 2 layers of CFRP of thickness of 0.111 mm/layer. The interfacial stiffness k_s of the adhesive was chosen to be 160 MPa/mm and held constant in this case. The load at initiation of macro debonding and the corresponding FRP strain were recorded. The effective bonding length of each beam was identified.

To investigate the parameters which affect the effective bonding length, the following main parameters were taken into consideration:

1. The interfacial stiffness k_s of the adhesive in which five values of 40, 80, 160, 320, and 640 MPa/mm were investigated. The interfacial stiffness was changed by changing the relative slip at the peak shear stress.
2. The reinforcing stiffness ($E_{frp}.t_{frp}$) where t_{frp} had the values of 0.111, 0.222, and 0.333 mm while E_{frp} held constant of 230 GPa which corresponds to $E_{frp}.t_{frp}$ of 25.53, 51.06, and 76.59 GPa mm respectively.
3. The fracture energy of the adhesive G_f^b in which the values of 0.6, 1.2, 1.8 were investigated. The fracture energy was changed by changing the ultimate relative slip, while the interfacial stiffness ks and the peak shear stress were held constant.
4. Shear-span ratio as discussed above in the first case.
5. Span length at constant shear-span ratio, where three beams of spans 2400, 4800, and 7200 mm having a shear-span ratio of 6.0 were investigated. The steel reinforcement ratio of each beam was held constant.

A beam of clear span of 2400 was selected to investigate the first three parameters. The effective bonding length of each case was identified.

RESULTS AND DISCUSSIONS

The effect of the shear-span ratio on the debonding behavior

Look at Figure 6, one can observe that for all investigated beams of shear-span ratios of 4.5, 6.0, 7.5, 9.0, and 12.0, the bending moment at the initiation of macro debonding is approximately constant which in return means that shear-span ratio has no significant effect on mode-II debonding initiation. That is an acceptable result because mode-II debonding is mainly dependant on the axial stress of FRP. Figure 7 exhibits the FRP stress distributions at the initiation of macro debonding for the different beams. Irregular behavior of the stress distribution curves may be attributed to crack spacing of 40mm, but this has insignificant effect on the accuracy of the results. Because we employed a constant cross section and a constant reinforcement ratio for all the beams in this case, the axial stress of FRP is dependent only on the bending moment. It is worth

mentioning that shear-span ratio may have significant effect on mode-I debonding, but this is still under investigation and out of scope of this paper.

Basic parameters affecting the effective bonding length

It is well known that the effective bonding length for a joint in the simple shear test is defined as the length beyond which no further increase in failure load can be achieved. Also, the initiation of macro debonding is considered as a type of failure, even if there is some gain in the ultimate strength after initiation of macro debonding, that gain will be insignificant. Based on these two points and without lack of generality, the effective bonding length of the investigated beams may be considered as shown in Figure 8 after approximating the FRP stress distributions to bilinear curve.

Mesh sensitivity -- To check the sensitivity of the identified effective bonding length to mesh size, three different mesh sizes were investigated, 5*5, 10*10, and 20*20 mm. Referring to Figure 9, it is obvious that mesh size has no significant effect on the identified effective bonding length and hence mesh size of 10*10 mm will be adopted through this study.

As stated above, to investigate the parameters which affect the effective bonding length, the following main parameters were taken into consideration:

1. The interfacial stiffness k_s.
2. The reinforcing stiffness (E_{frp}. t_{frp}).
3. Fracture energy of the adhesive layer.
4. Shear-span ratio.
5. Span of the beam.

In the following section, every parameter will be discussed in detail.

Interfacial stiffness K_s -- It is well known that if the interfacial stiffness of the adhesive is relatively high, this will cause rapid transfer of stresses from concrete to FRP and consequently results in delaying yielding of steel reinforcements, Niu and Wu (2002). Figure 10 shows the FRP stress distributions for the investigated beams having Ks values of 40, 80, 160, 320, and 640 MPa/mm. The identified effective bonding lengths are 4.55, 360, 330, 320, and 330 respectively. It is clear that for relatively small values of interfacial stiffness, the effective bonding length decreases as the interfacial stiffness increases. For values of interfacial stiffness higher than 160 MPa/mm, one can observe that interfacial stiffness has no significant effect on the effective bonding length. So, using adhesive having low interfacial stiffness will cause an increase to the effective bonding length which in return means relieving the stress concentration in the FRP and consequently delaying the debonding failure.

Effect of (E_{frp}.t_{frp}) -- To study the effect of the FRP reinforcing stiffness ($E_{frp}t_{frp}$) on the effective bonding length, three RC beams of clear span of 2400mm retrofitted with one, two, and three layers of FRP were investigated. The corresponding values of FRP reinforcing stiffness ($E_{frp}t_{frp}$) are 25.53, 51.06, and 76.59 GPa mm respectively. Figure 11

shows the FRP stress distributions for the investigated beams. It is clear that as the FRP reinforcing stiffness ($E_{frp}.t_{frp}$) increases, the effective bonding length increases.

Effect of of the fracture energy of the adhesive G_f^b -- Figure 12 shows the FRP stress distributions for the investigated beams having G_f^b of 0.6, 1.2, and 1.8. Using the method described previously in Figure 8, effective bonding length of 240, 330, and 430 mm respectively are obtained. As shown in Figure 13, as the fracture energy increases the effective bonding length increases.

Effect of shear-span ratio -- Figure 7 shows the FRP stress distributions for the investigated beams having clear spans of 1800, 2400, 3000, 3600, and 4800 which are corresponding to shear-span ratios of 4.5, 6.0, 7.5, 9.0, and 12.0 respectively. Adopting the method described previously for identifying the effective bonding length after approximating the FRP distribution curve to a bilinear one, effective bonding lengths of 230, 330, 410, 480, and 690 mm respectively can be obtained easily. It is clear that as the shear-span ratio increases, the effective bonding length increases. Figure 14 illustrates this relation which may be approximated to a straight line.

Effect of span -- Another factor which may affect the effective bonding length is the span at constant shear-span ratio. Keeping the shear-span ratio constant of 6.0, three beams of spans of 2400, 4800, and 7200 were solved. Figure 15 shows the FRP stress distributions for the investigated beams. Effective bonding lengths of 230, 350, and 610 may be obtained respectively. It is clear that as the span increases, the effective bonding length increases as indicated in Figure 16.

CONCLUSIONS

Based on finite element analysis and nonlinear fracture mechanics, the effect of shear-span ratio on the debonding behavior as well as factors affecting the effective bonding length of FRP-retrofitted RC beams was investigated. The following conclusions may be drawn:

1. The shear-span ratio has no significant effect on mode-II debonding initiation.
2. As the shear-span ratio increases, the effective bonding length increases. Increasing the span length while holding the shear-span ratio constant causes an increase in the effective bonding length. This has an implication that beams having larger spans and larger shear-span ratios after initiation of macro debonding may gain more loads before final failure.
3. Using adhesive having low interfacial stiffness will cause an increase to the effective bonding length which in return means relieving the stress concentration in the FRP and consequently delaying the debonding failure.
4. Using adhesive having high fracture energy may increase the effective bonding length and consequently delays the final failure after the initiation of macro debonding.
5. As the FRP reinforcing stiffness ($E_{frp}t_{frp}$) increases, the effective bonding length increases.

REFERENCES

ACI Committee 440.2 R-02 (2002), Guide for the Design and Construction of Externally Bonded FRP Systems for Strengthening Concrete Structures.

Ahmed, O., Van Gemert, D. and Vandeewall, L. (2000), *Improved Model for Plate-End Shear of CFRP Strengthened R.C. Beams*, Journal of Cement and Concrete Composites.

Bizindavyi, L. and Neale, K. W. (1999), Transfer lengths and bond strengths for composites bonded to concrete, *ASCE Journal of Composites for Construction*, 3(4), pp. 153-160.

Chen, J. F. and Teng, J. G. (2001), *Anchorage Strength Models for FRP and Steel Plates Attached to Concrete,* Journal of Structural Engineering, ASCE, Vol. 127, No. 7, pp. 784-791.

Faella C., Martinelli E., and Nigro E. (2004). Debonding in FRP strengthened RC beams: comparison between code provisions, *FRP Comosites in Civil Engineering-CICE 2004,* pp. 189-197**.**

fib: Bulletin d'information n. 14 (2001), *Externally bonded FRP reinforcement for RC structures.*

Hillerborg, A.; Modeer, M.; and Petersson, P.E., (196), *Analysis of Crack Formation and Crack Growth in Concrete by Means of Fracture Mechanics and Finite Elements,* Cement and Concrete Research, pp. 773-782.

DIANA-8.1 User's Manual, TNO Building and Construction Research, Lakerveld b.v., The Hague, 2003.

JSCE (2001), Recommendation for upgrading of concrete structures with use of continuous fiber sheets, Concrete Engineering Series 41.

Lorenzis, L. D., Miller, B. and Nanni, A. (2001), Bond of FRP laminates to concrete, *ACI Materials Journal*, 98(3), pp. 256-264.

Malek, A. M., Saadatmanesh, H. and Ehsani, M. R. (1998), Prediction of failure load of R/C beams strengthened with FRP plate due to stress concentration at the plate end, *ACI Structural Journal*, 95(1), pp. 142-152.

Morita, S.; Muguruma, H.; and Tomita, K. (1967), *Fundamental Study on Bond between Steel and Concrete,* Transaction of AIJ, 131(1), pp.1-8.

Nakaba, K., Kanakubo, T., Furuta, T. and Yoshizawa, H. (2001), Bond behavior between fiber-reinforced polymer laminates and concrete, *ACI Structural Journal*, 98(3), pp. 359-367.

Niu, H. and Zhishen Wu (2002), *Strengthening Effect of RC Flexural Members with FRP Sheets Affected by Adhesive Layers,* Journal of Applied Mechanics, Vol. 5, pp. 887-897.

Roberts, T. M. (1989), Approximate analysis of shear and normal stress concentrations in the adhesive layer of plated RC beams, *The Structural Engineer*, 67(12), pp. 229-233.

Sato, Y., Asano, Y. and Ueda, T. (2000), Fundamental study on bond mechanism of carbon fiber sheet, *JSCE Journal of Material, Concrete Structures and Pavements*, 47(648), pp. 71-87 (in Japanese).

Täljsten, B. (1997), Strengthening of beams by plate bonding, *ASCE Journal of Materials in Civil Engineering*, 9(4), pp. 206-212.

Triantafillou, T. C., and Plevris, N., (1992), *Strengthening of RC Beams with Epoxy-Bonded FRP Composite materials,* Materials and Structures, V. 25, pp. 201-211.

Wu, Z. S. Matsuzaki, T., and Tanabe, K., (1998), *Experimental Study on Fracture Mechanism of FRP-Reinforced Concrete Beams,* Proceeding of JCI Symposium on Non-metallic FRP Reinforcement for Concrete Structures, pp. 119-126.

Wu, Z. S. and Yin, J. (2002), *Numerical analysis on interfacial fracture mechanism of externally FRP-strengthened structural member,* JSCE Journal of Material, Concrete Structures and Pavements, 55(704), pp. 257-270.

Yaun, H. and Wu, Z.(1999), *Interfacial Fracture Theory in Structures Strengthened with Composite of Continuous Fiber,* Proceedings of Symposium of China and Japan, Science and Technology of 21st Century, Tokyo, Japan, pp. 142-155.

Yoshizawa, H., Wu, Z. S., Yuan, H. and Kanakubo, T. (2000), *Study on FRP-concrete interface bond performance*, JSCE Journal of Material, Concrete Structures and Pavements, 49(662), pp. 105-119.

Ziraba Y.N., Baluch M.H., Basunbul I.A., Sharif A.M., Azad A.K. and Al-Sulaimani G.J. (1994), *Guidelines toward the Design of Reinforced Concrete Beams with External Plates*. *ACI Structural Journal* 91(6), pp. 639-646.

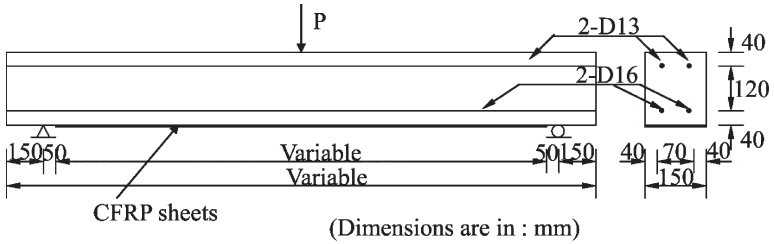

Figure 1—Details of the simulated beam.

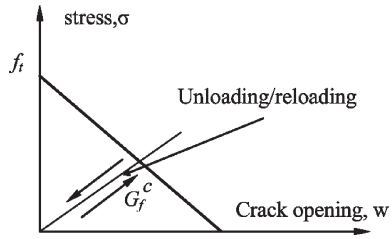

Figure 2 —Linear tension softening model for concrete.

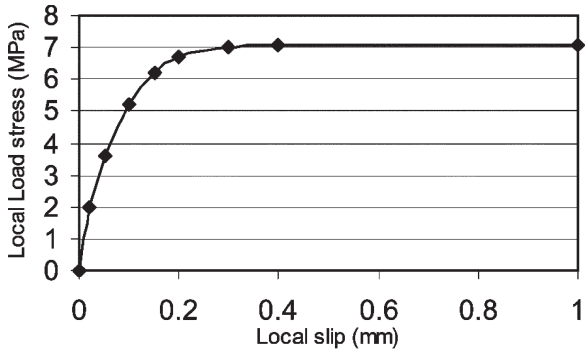

Figure 3—Bond-slip model for steel-concrete interface (Morita et al., 1967).

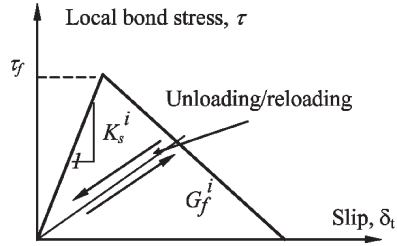

Figure 4—Linear softening model for FRP-concrete interface.

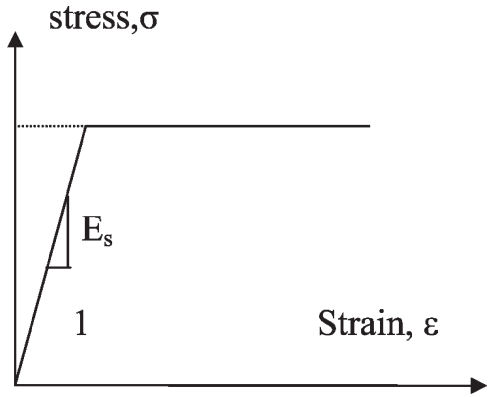

Figure 5—Elastic-perfectly plastic model for steel reinforcement.

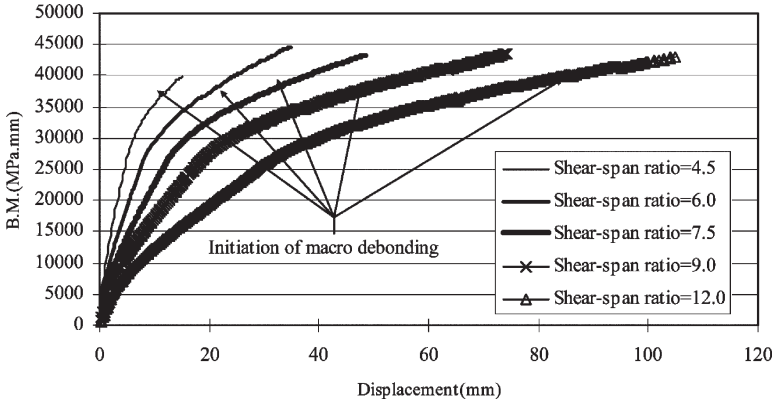

Figure 6—Mid-span displacement versus mid-span B.M. for different shear-span ratios.

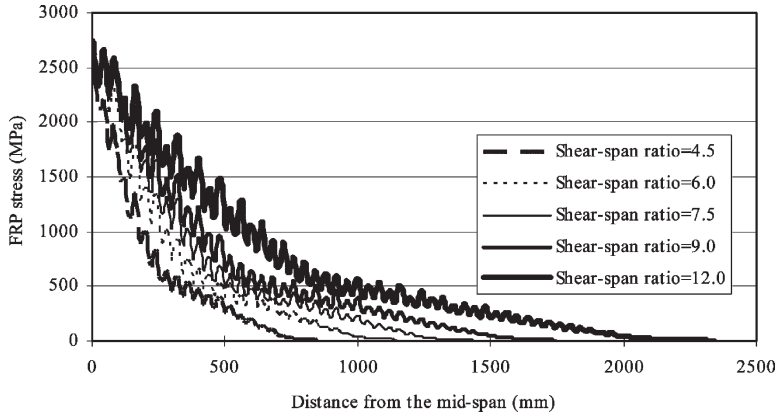

Figure 7—FRP stress distribution for different shear-span ratios at initiation of macro debonding.

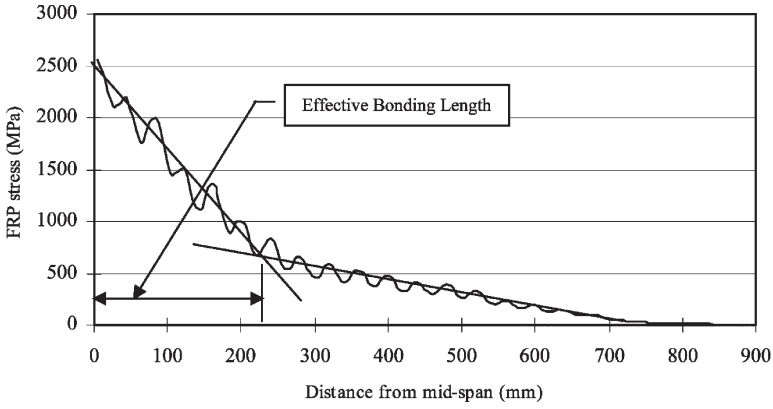

Figure 8—Suggested method for identifying the effective bonding length.

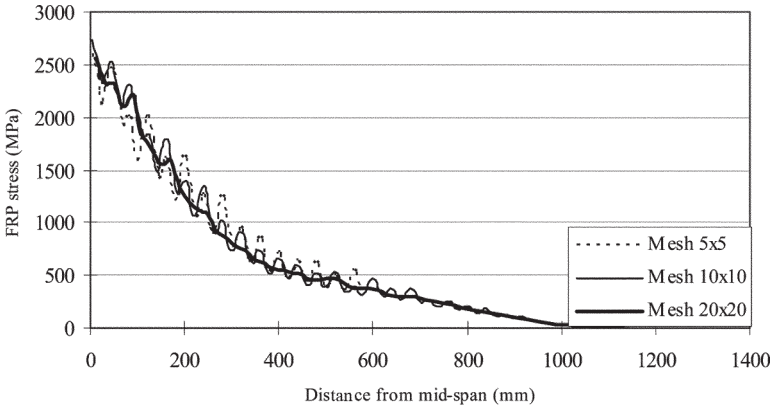

Figure 9—Sensitivity of the effective bonding length to the mesh size.

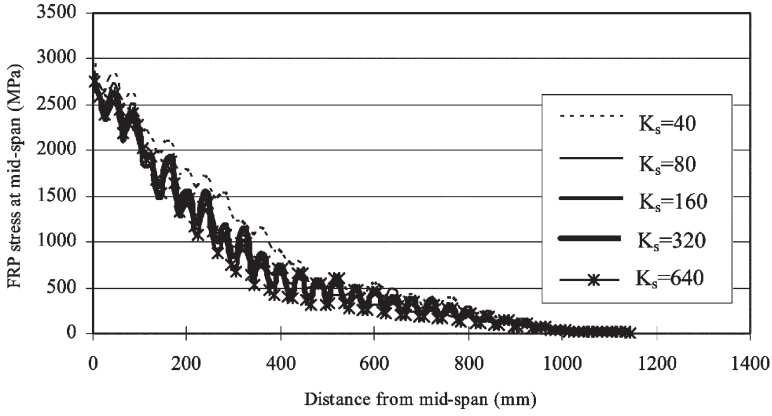

Figure 10—FRP stress distribution for different interfacial stiffness at initiation of macro debonding.

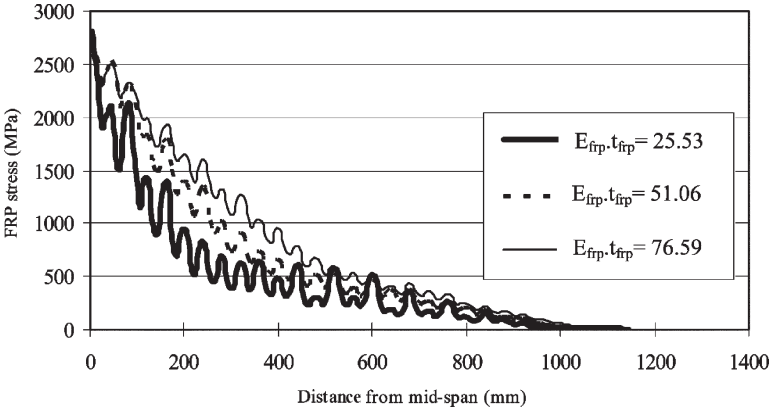

Figure 11—FRP stress distribution for different values of FRP reinforcing stiffness ($E_{frp}.t_{frp}$) at initiation of macro debonding.

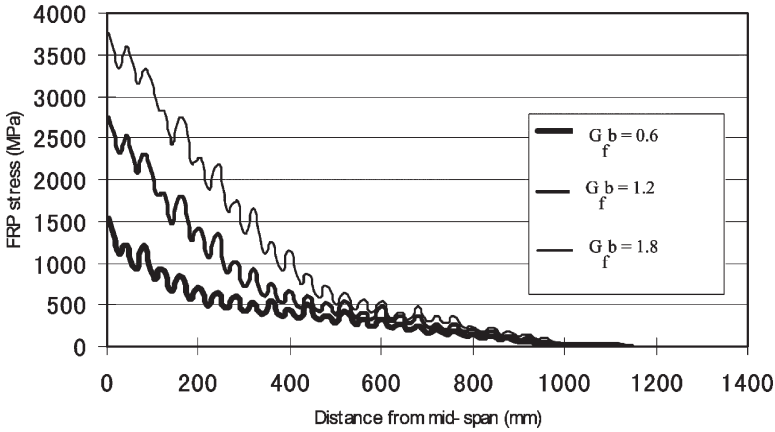

Figure 12—FRP stress distribution for different values of fracture energy of adhesive at initiation of macro debonding.

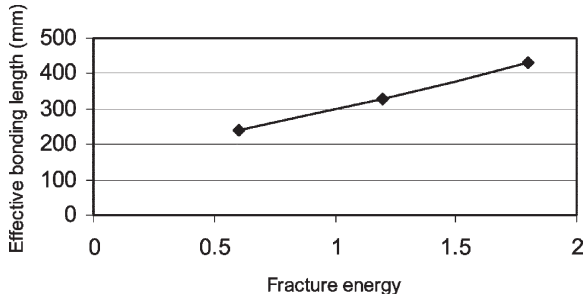

Figure 13—Relation between fracture energy of adhesive and effective bonding length.

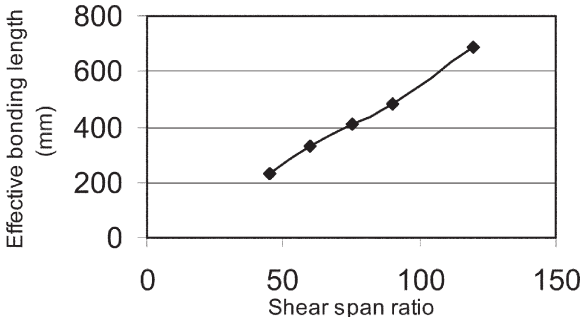

Figure 14—Relation between shear-span ratio and effective bonding length.

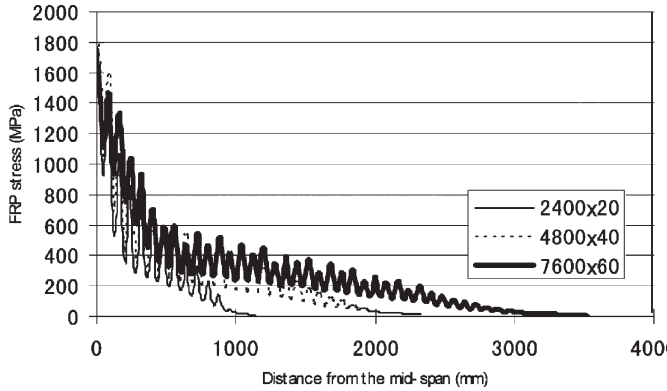

Figure 15—FRP stress distribution for different values of spans with a constant shear-span ratio at initiation of macro debonding.

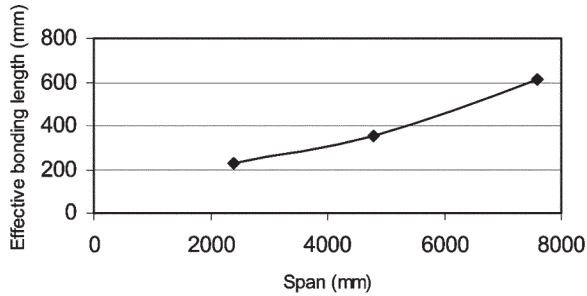

Figure 16—Relation between span and effective bonding length.